Artificial Neural Network Optimization of Adsorption Parameters for Cr(VI), Ni(II) and Cu(II) Ions Removal from Aqueous Solutions by Riverbed Sand

Kavitha; B.*[+•]

PG and Research Department of Chemistry, Cardamom Planters' Association College, Bodinayakanur, Tamilnadu, INDIA

Sarala Thambavani; D.[•]

Department of Chemistry, PRIST University, Madurai, Tamilnadu, INDIA

ABSTRACT: *Removal of Cr(VI), Ni(II), and Cu(II) from aqueous solution by Riverbed Sand containing Quartz as major clay minerals as a non-toxic and economically viable treatment was investigated. The structure, morphology, surface area, and elemental composition were confirmed using XRD, SEM, EDAX, FT-IR, and BET techniques. The N_2 adsorption-desorption isotherm reveals their mesoporous structure and large BET surface area (122.75 m^2/g). The effect of the initial metal concentration, pH, adsorption dosage, contact time, and temperature were examined in batch experiments to understand adsorption isotherms, kinetics, and thermodynamics. Results suggest that the equilibrium adsorption was described by the Langmuir model. Adsorption kinetics was described well by the pseudo-second-order model and were followed by an intraparticle diffusion mechanism. The thermodynamics studies reveal that the adsorption was spontaneous and exothermic. An Artificial Neural Network (ANN) model was used to optimize the removal efficiency of Cr(VI), Ni(II), and Cu(II) on QKCI. The model was developed using a three-layer feed-forward backpropagation algorithm with 15, 18, and 20 hidden neurons for Cr(VI), Ni(II), and Cu(II) ions. Comparison between the model results and experimental data gives a high degree of correlation (R^2= 0.9863 for Cr(VI), 0.9591 for Cu(II)) and 0.9469 for Ni(II) indicating that the model is able to predict the sorption efficiency with reasonable accuracy.*

KEYWORDS: *Adsorption; Isotherm; Kinetics; Thermodynamics; Artificial neural network models.*

INTRODUCTION

Heavy metals, released into the environment through anthropogenic sources have been increasing constantly and their persistency as well as non-biodegradability poses a serious threat because of their carcinogenic and mutagenic effects to the living organism [1]. The sustainability of any human community hingeson

* *To whom correspondence should be addressed.*

+ *E-mail: kaviravee@gmail.com*

• *Other Address: Research and Development Centre, Bharathiar University, Coimbatore, INDIA*

1021-9986/2020/5/203-223 21/$/7.01

an adequate supply of potable water, which confirms to the acceptable standard. This makes removal of heavy-metal ions in waste water an essential factor for environmental and human health protection. Heavy-metal ions such as Cr(VI), Ni(II) and Cu(II) usually present in industrial effluents posses the serious problem to the human health [2- 6]. For instance, Cr(VI)causes acute toxicity, irritation and ulceration of the nasal septum, asthma, systemic poisoning damage or even severe burns and interference with the healing of cuts or scrapes, which may lead to ulceration and chronic allergic contact dermatitis and effect's kidney and liver functions [7]. Cu(II) leads to Wilson's disease, mucosal irritation, hepatic and rental damage, central nervous problem lung cancer [8 - 10]. Presence of Ni(II)in consumed water may cause serious harm to the kidneys, lungs and the skin [11]. Various techniques have been employed for removal of heavy metals, including precipitation, adsorption, ion exchange membrane separation and reverse osmosis [12]. Adsorption is widely used to remove heavy metals from water due to the availability of wide range of adsorbents, the comparatively low cost of application and the ease of operation [13]. Activated carbon has been the most popular adsorbent due to its high surface area, high adsorption capacity and high degree of surface reactivity [14]. However, the application of activated carbon for waste-water treatment is not feasible due to it high price and cost associated with the regeneration. Natural clays are relatively cheap, exhibit higher adsorption capacities, low-cost and readily available materials functioning as excellent exchangers, which have often been used to adsorb metallic contaminants [15]. Clay is composed mainly of silica, alumina and water, frequently with appreciable quantities of iron, alkali metals and alkaline earth earths [16]. Clay's materials possess a layered structure and are classified by the differences in their layered structures. Two structural units are involved in the atomic lattices of most clay minerals. One unit consists of closely packed oxygen and hydroxyl in which aluminium, iron and magnesium atoms are embedded in an octahedral combination so that they are equidistant from six oxygens or hydroxyls [17]. The second unit is built of silica tetrahedrons. The silica tetrahedrons are arranged to form a hexagonal network that is repeated indefinitely to form a sheet of composition, $Si_4O_6(OH)_4$[18]. Riverbed Sand has the potential to sequester heavy-metal ions from solutions. Abundant availability, high sorption capacity, cost-effectiveness, high cation exchange capacity and renew ability are the important factors making these materials as economic alternatives for water treatment and waste remediation [19-21]. Riverbed Sand containing Quartz has been used throughout this research due to its ion-exchange capacity, availability, excellent surface and structural properties compared to commercial clays.

Heavy-metal removal using the adsorption process is a complex process because a large number of variables influence the removal efficiency. Modeling of such a process is difficult when a standard procedure like simple linear multivariate correlation is used [22]. The Artificial Neural Network (ANN) method is a modeling method that can introduce mathematical functions for both linear and non-linear systems. ANN's are applicable to solve wide range of problems, including a requirement to the high number of experiments and consumption of chemical reagent, especially in complex systems. It is composed of simple computational units (neurons) that are connected in a parallel structure which are inspired by biological neurons in the human brain [23]. This technique is superior to conceptual models in terms of higher speed, simplicity and large-capacity [24].Therefore, the use of ANN to optimize the factor that strongly affect the removal of heavy metals fordeveloping a phenomenological mathematical model as a metal ion removal process is scare in the literature. To the best of our knowledge, although ANN was applied to model biosorption [25], adsorption [26], photo electron-Fenton [27] photocatalysis [28], and ANN modeling of removal of Cr(VI), Ni(II) and Cu(II) using Quartz was not discussed.

In this study, the removal of Cr(VI), Ni(II) and Cu(II) from aqueous solution using abundantly available, cost-effective and renewable material Riverbed Sand containing Quartz as the adsorbent by batch adsorption technique was investigated. Equilibrium and kinetic studies were tested to describe the adsorption process. Different models were tested to determine the rates and mechanisms of the adsorption process. The thermodynamic parameters were determined using van't Hoff equation. In addition, an ANN model with their larger is developed to optimize the removal efficiency of Cr(VI), Ni(II) and Cu(II) from aqueous solution by Quartz clay minerals.

EXPERIMENTAL SECTION

Materials

Aqueous solution of ions at various concentrations were prepared from $K_2Cr_2O_7$, $NiSO_4.6H_2O$ and $CuSO_4.5H_2O$ were used as sources of Cr(VI), Ni(II) and Cu(II) respectively. All other reagents and solvents were of analytical grade reagents and used without further preparation of adsorbent and adsorbate purification.

Collection of Riverbed Sand

Suruli falls is a famous tourist attraction located in Theni District in Tamil Nadu. It is 56 kms from Theni and 10 kms from Cumbum. Madurai is almost 123 kms away from the falls and it lies on the way to Periyar National Park. Suruli falls is located in between 9°39′52″ north latitudes and 77°18′12″ east longitude. Suruli River, the mouth of the falls originates from the Meghamalai Mountain range. The soil samples were collected from Suruli river named as Suruli Theertham, Theni District, Tamilnadu, India.

For the adsorption studies of heavy metal ions freshly deposited sand near the river bank were collected in polyethylene bags from the upstream section of the river and brought to the laboratory. Samples were taken from the upper 5 cm of the sediments at places where flow rates were low and sedimentation was assumed to occur. The soil samples were initially sun dried for 7 days followed by drying in hot air oven at 383±1 K for 2 days. The dried soil was crushed, sieved (using 150 mm mesh size) and then stored in sterile, closed glass bottles till further investigation [29].

Zero point charge

The zero point charge (pH) for the adsorbent was determined by introducing 1.0 g of Riverbed Sand into six 100 mL Erlenmeyer flasks containing 100 mL of 0.1 M potassium nitrate solution. Initial pH values of the six solutions were adjusted to 2, 4, 6, 8, 10 and 12 by either adding few drops of nitric acid or potassium hydroxide. The solution mixtures were allowed to equilibrate in an isothermal shaker (25±1°C) for 24 h. Then the suspension in each sample was filtered and the final pH was measured again. The procedure was repeated by varying the mass of Riverbed Sand introduced into the solution from 0.1-1.0 g. The value of pH_{ZPC} can be determined from the curve that cuts the pH 0 line of the plot Δ pH versus pH_0.

Characterization of Riverbed Sand

The FT-IR studies of the collected Riverbed Sand adsorbent were characterized using a JASCO spectrophotometer with KBr pelletisation in a wide range wavelength ranging from 400 cm^{-1} and 4000 cm^{-1}. Scanning electron microscope (JEOL JSM – 6100) was used to study the surface morphology of the adsorbent at the required magnification at room temperature. The chemical composition was determined by an Energy Dispersive X-ray Spectroscopy (EDAX) attached to SEM. The X-ray diffraction (XRD) of the samples was carried out on XPERT PRO PANI analytical X-ray diffractometer using Ni filtered Cu Kα radiation with a scanning angle (2θ) of 20-100 °C. The surface area was measured on approximately 250 mg of the samples using Kr at the liquid nitrogen temperature using a Micromeritics ASAP 2020 apparatus. Before the measurements, the samples were degassed at 350°C for 18 h. The values of the surface areas were determined by the Brunauer–Emmet–Teller (BET) analysis of the physisorption isotherms.

Batch adsorption studies

Batch adsorption studies were performed using different concentration of potassium dichromate, copper sulphate and nickel sulphate. The extent of metal ion removal was investigated separately by changing the adsorption dose, pH of the solution, contact time, agitation speed and temperature of the adsorbent metal solution mixtures. Metal stock solutions were diluted to required concentrations for obtaining solutions containing 10-100 mg/L of Cr(VI), Cu(II) and Ni(II) ions. Batch experimental studies were carried out with a known weight of adsorbent and 200 ml of Cr(VI), Cu(II) and Ni(II) solution of the 10 mg concentration at an optimum pH in 250 mL RB flasks. The flasks were stirred at 500 rpm. After attaining the equilibrium adsorbent was separated by filtration using Whatman filter paper and the aqueous-phase concentration of metal was determined by UV-Vis spectrophotometer. The concentration of chromium left in the solution was determined by the standard spectrophotometric method using diphenyl carbazide as the complexant for chromium. Diphenyl carbazide reacts with Cr(VI) in acidic medium to give a red-violet complex at 540 nm. The color intensity is proportional to the concentration of Cr(VI) in the solution, Nickel reacts with dimenthyl glyoxime in the presence of an alkaline

oxidizing agent to form a characteristic red colour complex which was measured spectrophotometrically at 470 nm and The copper ion concentration in the liquid phase was determined spectrophotometrically by making a complex with sodium diethyl dithiocarbamate at 435 nm respectively.The percentage adsorption was determined using the equation:

$$\% \text{ Adsorption} = \frac{C_0 - C_e}{C_0} \times 100 \quad (1)$$

Where C_0 and C_e are the initial and equilibrium concentration of metal ion solution (mg/L). The amount of for Cr(VI), Cu(II) and Ni(II) ions (q_e) adsorbed per unit mass of QKCI was calculated using the equation:

$$q_e = \frac{(C_0 - C_e)\ V}{m} \quad (2)$$

Where C_o and C_e is the initial and equilibrium concentration of metal ion solution (mg/L), respectively, V is the volume of the solution in liter (L) and m is the amount of Riverbed Sand in grams (g).

Desorption studies

The adsorption is reversible in some cases, adsorbents can be regenerated through desorption. Desorption studies were performed using tap water (pH 7) and HCl solutions. These experiments were carried out by immersing the metal ion-loaded Riverbed Sand in 30 mL of tap water and diluted acid solutions for 4 h at a static speed. The filtrate was collected and analyzed in UV – Vis Spectrophotometer. The percentage of desorption was calculated by the following expression:

$$\% \text{ Desorption} = \frac{m_d}{m_a}$$

Where m_d is the amount of metal ion desorbed (mg/L) and m_a is the amount of metal ion adsorbed (mg/L).

Definition of the ANN model

ANN, biologically inspired network algorithms has attracted increasing attention recently. It is a flexible mathematical structure which is capable of identifying complex nonlinear relationships between input and output data sets. The multilayer feed forward neural network, also known as MultiLayer Percepton (MLP) is widely applied neural network architecture (Fig.1) to solve nonlinear regression problem [30]. The ANN model in this work is consisted of three layers such as input, hidden and output layers. The layers, number of neurons as processing unit of ANN in each layer and the transfer functions between layers form neural network topology [31]. The linear transfer function was used in hidden and output layers. Initial metal ions concentration, pH, adsorbent dosage, contact time, agitation speed and temperature were used as input to the ANN model. 91 experimental data points were used to feed the ANN structure. The samples were allocated to training, test and validation sets that contains75 %, 15 % and 15 % samples, respectively. The complete data normalized in the 0–1. Therefore, data (X_i) are converted to a normalized value (X_{normal}) as follows [32, 33]:

$$X_{normal} = \frac{X_i - X_{min}}{X_{max} - X_{min}} \quad (3)$$

X_{min} and X_{max} are minimum and maximum actual experimental data. The input signals are modified by interconnection weight known as weight factor (W_{ij}), which represents the interconnection of i^{th} node of the first layer to j^{th} node of the second layer. The sum of modified signals (total activation) is then modified by a sigmoid transfer function and output is collected at the output layer [34]. In order to evaluate the integrity of the fit of experimental data and the prediction accuracy of the models utilized in the present work, the following statistical indices are employed [35]:

$$MSE = \sum \frac{\left|\left(q_{exp} - q_{cal}\right)/q_{exp}\right| * 100}{N} \quad (4)$$

The network is tested with different number of neurons to find the optimum number of neurons at hidden layer by observing the mean squared error (MSE). The lowest mean square error is shown for 15, 18 and 20 neurons and also maximum R-square is obtained for 15, 18 and 20 neurons for Cr(VI), Ni(II) and Cu(II) respectively.

RESULTS AND DISCUSSION

Characterization of Riverbed Sand

The typical FT-IR spectrum of Riverbed Sand is shown in Fig.2. In the FT-IR studies of the Riverbed Sand, the Si-O stretching vibration were observed at 779.2 cm^{-1}, 694.4 cm^{-1}, 540.1 cm^{-1} and 447.5 cm^{-1} showing the presence of quartz [36]. The bands at 3699.5 cm^{-1}, 3425.5 cm^{-1}, 1033.8 cm^{-1}, 694.4 cm^{-1}, 540.1 cm^{-1} and 447.5 cm^{-1} shows the presence of kaolinite [37]. The vibration observed at 694.4 cm^{-1} shows the possibility of the presence of chlorite [38].

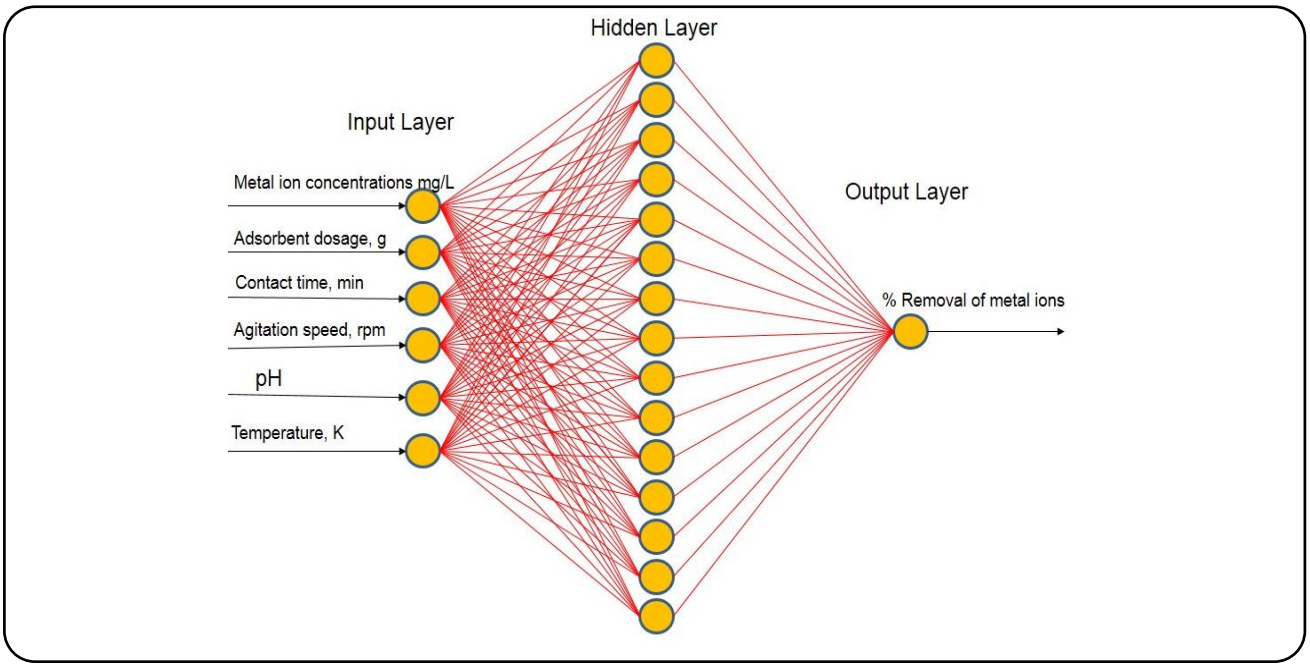

Fig. 1: The ANN architecture.

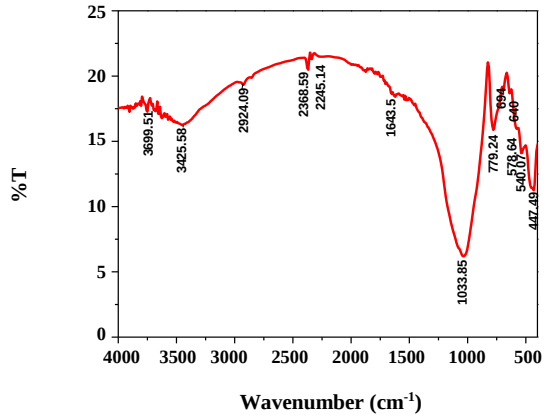

Fig. 2: FT-IR spectrum of Riverbed Sand.

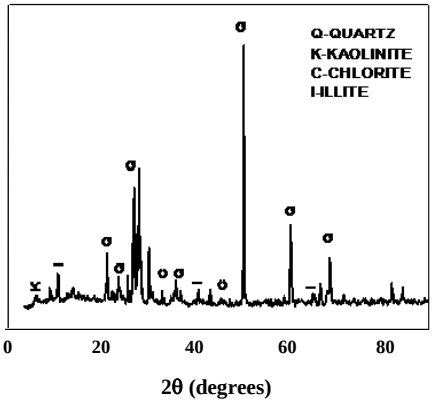

Fig. 3: XRD pattern of Riverbed Sand.

The presence of bands at 3699.5 cm^{-1}, 3425.5 cm^{-1}, 2368.5 cm^{-1} and 1033.8 cm^{-1} and 779.2 cm^{-1} indicate the presence of illite. The presence of chlorite was confirmed by a band at 3425.5 cm^{-1} and the band at 1643.5 cm^{-1} indicates the presence of iron content. XRD pattern of QKCL (Fig. 3) was used to confirm the presence of clay minerals such as quartz, kaolinite, chloriteand illite. The d-values of Riverbed Sand was compared with standard values of clay minerals supplied by crystallographic and crystallo chemical database for minerals and their structural analogues compared. It can be concluded that the Riverbed Sand is mainly quartz containing small amount of kaolinite, trace amount of chlorite and illite. The SEM micrographs of the Riverbed Sand were shown in Fig. 4. It depicts the platy flakes and spongy structure of the Riverbed Sand. EDAX spectrum was used to find out the type of elements present in the Riverbed Sand. The microanalysis spectrum of the Riverbed Sand was depicted in Fig. 5. The result indicated the presence of silica, alumina, iron, calcium, sodium and potassium oxide as major constituents, while the other oxides such as magnesium oxide, manganese oxide and phosphorous pentaoxide were present in smaller amount. Therefore the adsorbate species in solutions were expected to be removed

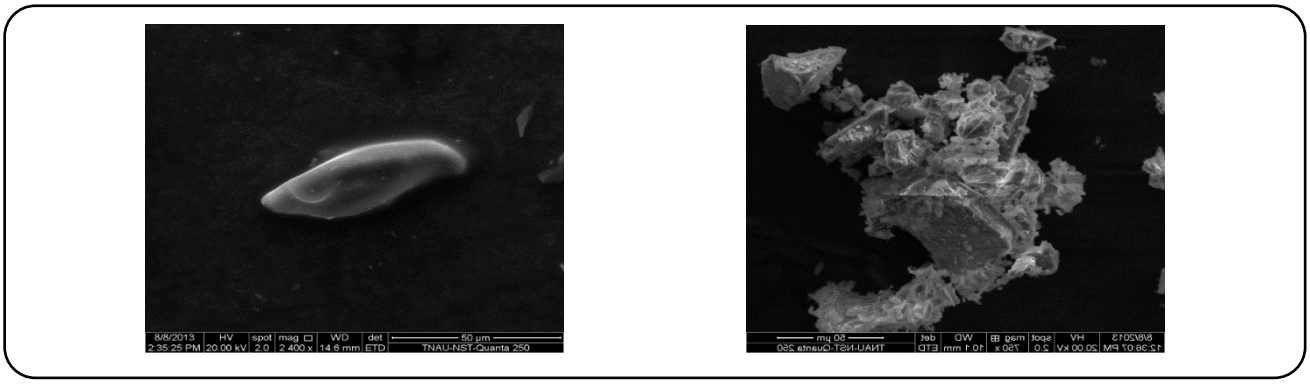

Fig. 4: SEM images of Riverbed Sand at high and low magnification.

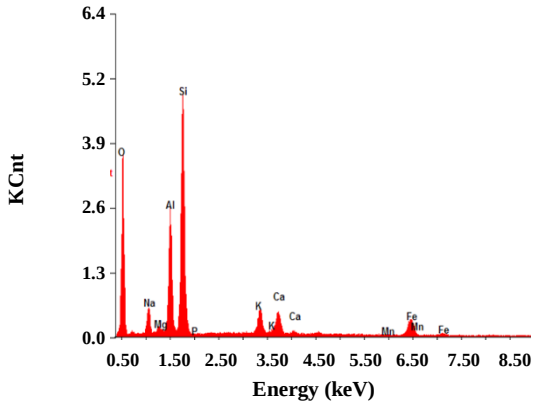

Fig. 5: EDAX spectrum of Riverbed Sand.

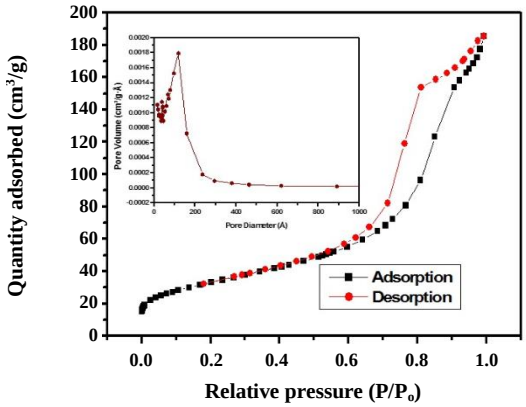

Fig. 6: BET surface area of Riverbed Sand.

mainly by SiO_2 and Al_2O_3. N_2 adsorption-desorption isotherms was used to investigate the surface area of Riverbed Sand and shown in Fig.6. The BET surface area Riverbed Sand is 122.75 m²/g. This is a high value, high specific surface area and abundant mesopores are desirable features for adsorption. Fig. 6 also presents Barret-Joyner-Halenda (BJH) pore size distribution curve (in the inset) of the figure with pore size of 92.588 Å.

Effect of pH

The solution pH in adsorption experiments is one of the most important parameters that is effective on the solution chemistry and metal speciation and uptake capacity adsorbent functional groups activity and adsorption mechanism. It is directly related to the competition ability of hydrogen and metal ions to the adsorbent surface active site [39]. In this work the effect of pH on the adsorption of Cr(VI), Ni(II) and Cu(II) ions on Riverbed Sand was studied in the range of 2 to 10. The results were shown in Fig. 7 and indicate that the maximum removal percentage of Cr(VI), Ni(II) and Cu(II) was obtain at the pH 2,6 and 8 respectively. As observed the uptake levels of Cr(VI), Ni(II) and Cu(II) ions increased significantly with increasing pH from 2 to 6 for Cu(II) and 2 to 8 for Ni(II) respectively. The increase in both metal adsorption and pH values can be explained on the basis of competition between the proton and metal ions for the same terminal binding site on Riverbed Sand. At low pH values, the concentrations of H^+ ions exceeds that of the metal ions and hence H^+ ions compete with Cu(II) and Ni(II) ions for the surface of the adsorbent which would hinder the metal ions from reaching the binding sites of the adsorbent caused by repulsive forces. At high pH precipitation usually occurred between metal ions and hydroxide ions [40, 41]. At pH 7 for Cu(II) and 9 for Ni(II) precipitation were observed. In contrast the highest Cr(VI)adsorption was observed at pH 2. The adsorption capacity decreased sharply with an increase in solution pH above 2 under strong acidic conditions, Riverbed Sand were protonated to form the positively charged sites and electrostatic

Table 1: Physico-Chemical characteristics of Riverbed Sand.

Parameter	Value
pH	6.9
pH_{ZPC}	2.5
Specific surface area	122.7531 m^2/g
Cation exchange capacity	13.1 meq g−1
SiO_2	89.05 (%)
Al_2O_3	2.01 %
Fe_2O_3	3.1 %
CaO	0.56 %
MgO	3. 5 %
MnO	0.02 %
Na_2O	0.4 %
K_2O	1.6%
TiO_2	0.25 %

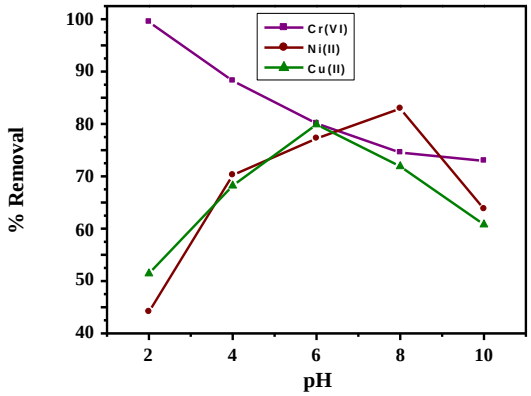

Fig. 7: Effect of pH on the adsorption of Cr(VI), Ni(II) and Cu(II) onto Riverbed Sand.

attraction occurred between Cr(VI)and Riverbed Sand leading to the increase of Cr(VI)removal efficiency. There are several forms of Cr(VI)ions existing in the aqueous solution such as chromate [CrO_4^{2-}], dichromate [Cr_2O7^{2-}] and hydrogen chromate [$HCrO_4^-$]. The relative amount of these ions depends on the pH and total chromate ions [$HCrO_4^-$] are the dominant species among the chromate ions. The results indicated that the maximum uptake of Cr(VI) ions takes place at lower pH [42]. The effect of pH can also be explained in terms of pH_{zpc} of Riverbed Sand. The point of zero charge is the point at which surface acidic and basic functional groups no longer contribute to the pH value of the solution. The pH_{zpc} of Riverbed Sand was found to be around 2.5 as shown in Table 1. Below pH 2.5 the surface is positively charged and the binding of metal ions tends to be low due to repulsive forces. Increasing the pH above pH_{zpc}, the surface of Riverbed Sand became negatively charged there by enhancing the metal ions adsorption.

Effect of concentration

A study of the effect of change in the amount adsorbed with concentration of Cr(VI), Ni(II) and Cu(II) was carried out keeping adsorbent dosage fixed and varying the concentration from 10 to 100 mg/L. Fig. 8 shows that he percentage removal of Cr(VI), Ni(II) and Cu(II) decrease as concentration of metal ions increases from 10 to 100 mg/L. With the increase in concentration of Cr(VI), Ni(II) and Cu(II) there will be less availability if adsorbent surface as assess the large number of Cr(VI), Ni(II) and Cu(II) ions on the surface will reduces [43].At low concentration, most of the metal ions in solution interact with active sites on adsorbent resulting in high percentage removal. At higher concentration, the studied metal ions remain unadsorbed as the active sites are saturated. Hence the percentage removal of Cr(VI), Ni(II) and Cu(II) depends on the initial metal ions concentration and decreases with increase in initial metal ions concentration.

Effect of adsorbent dosage on removal of metal ions

Fig. 9 shows the effect of adsorbent dosage on the removal efficiency of Cr(VI), Ni(II) and Cu(II) on Riverbed Sand. The amount of adsorbent was varied from 0.05 to 0.4 g. In this experiment the adsorptive ability of the adsorbents at a definite concentration of 10mg of Cr(VI), Ni(II) and Cu(II) was considered with increase in the amount of adsorbent up to 0.25 g for Riverbed Sand adsorption efficiency was found to increase. This may be due to an increase in number of active sites of the absorbent material with increasing amount of the adsorbent [44]. However further increase in the Riverbed Sand dosage leads to decrease in adsorption efficiency. It may be due to the overlapping of active sites at higher Riverbed Sand dosage [45]. So, 0.25 g Riverbed Sand was considered as optimum dosage and was used for further study.

Effect of contact time on the adsorption efficiency

The time to reach saturated adsorption is of great importance for evaluation the affinity of the adsorbent

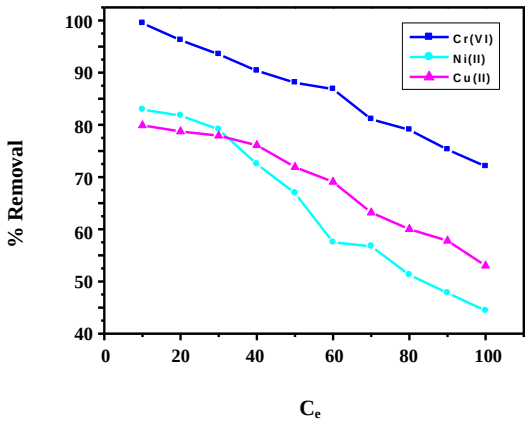

Fig. 8: Effect of concentration of metal ion solutions on the adsorption of Cr(VI), Ni(II) and Cu(II) onto Riverbed Sand.

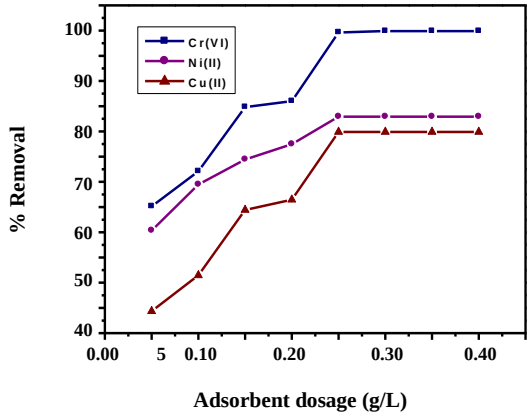

Fig. 9: Effect of adsorbent dosage on the adsorption of Cr(VI), Ni(II) and Cu(II) onto Riverbed Sand.

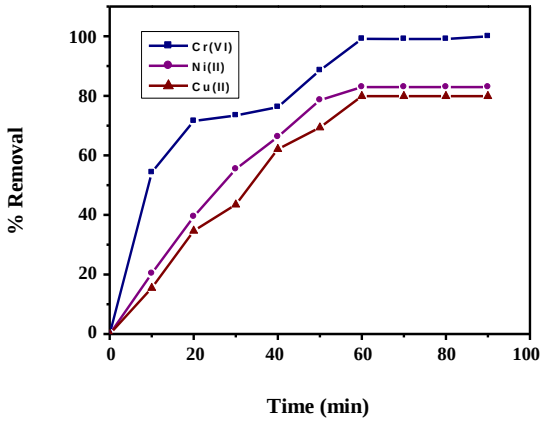

Fig. 10: Effect of contact time on the adsorption of Cr(VI), Ni(II) and Cu(II) onto Riverbed Sand.

to the Cr(VI), Ni(II) and Cu(II) ions. Therefore, the effect of the contact time on the adsorption of Cr(VI), Ni(II) and Cu(II) was studied and shown in Fig. 10. The Cr(VI), Ni(II) and Cu(II) removal increased rapidly at the beginning of adsorption with increasing contact time and there after attained to the equilibrium. After the adsorbing ions get adsorbed on the surface the capacity of the adsorbent get exhausted and the saturation adsorption capacity is reached [46]. The minimum contact time required to reach the equilibrium is found as 60 min for Riverbed Sand to Cr(VI), Ni(II) and Cu(II). The primary adsorption rate was very fast which was perhaps caused by the existence of a large number of adsorbent sites available for Cr(VI), Ni(II) and Cu(II) removal. When the surface areas decreased the adsorption rate slowed down, which may have been caused by the development of repulsive forces between the Cr(VI), Ni(II) and Cu(II) ions on the solid surface and those in the liquid phase.

Effect of agitation speed

In the adsorption systems for a given agitation speed the removal efficiency of a metal ion increases with increasing he contact time .Therefore agitation speed is a very important factor which strongly affects the equilibrium time therefore to investigate the effect of agitation speed on the adsorption of Cr(VI), Ni(II) and Cu(II) the adsorption studies were done at different agitation speed ranging from 0 (without agitation) to 800 rpm while keeping other experimental parameters constants. It was found that the removal efficiency increases with increase agitation speed 72.32 % to 99.48 % , 46.34 % to 82.92 % and 42.34 to 79.90 % for Cr(VI), Ni(II) and Cu(II) ions respectively (Fig. 11).Cr(VI), Ni(II) and Cu(II) removal gradually increases with increase in agitation speed from 100 to 500 rpm and then decrease to explain this trend it is worth mentioning that the mechanism of removal from aqueous solution involved four steps. The first step involved migration of Cr(VI), Ni(II) and Cu(II) ions from the bulk solution to the surface of the adsorbent. The second step involves diffusion through the boundary layer to the surface of adsorbent. The third steps involves adsorption at a site. The fourth steps involves intra-particle diffusion into the interior of the adsorbent. Increasing agitation speed decreases the boundary layer resistance of the transfer of Cr(VI), Ni(II) and Cu(II) ions from the bulk solution to the adsorbent surface.

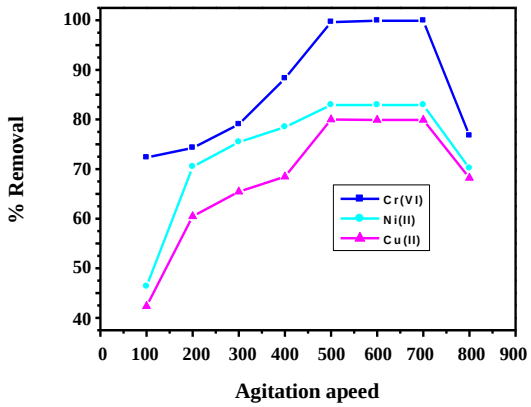

Fig. 11: Effect of agitation speed on the adsorption of Cr(VI), Ni(II) and Cu(II) onto Riverbed Sand.

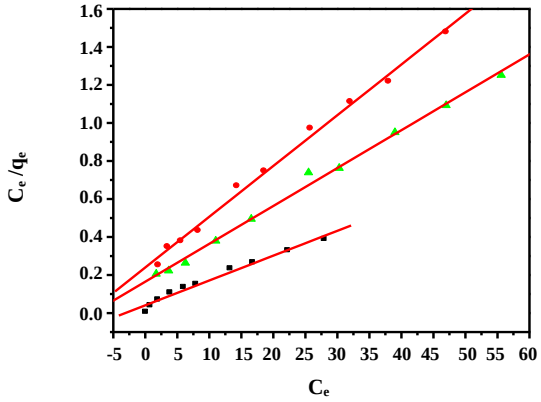

Fig. 12: Linear plot of Langmuir isotherm for adsorption of Cr(VI), Ni(II) and Cu(II) onto Riverbed Sand.

This adsorbate is forced towards the adsorbent surface and leads to an increase in the diffusion of adsorbate into the surface of the adsorbent [47, 48]

Effect of temperature

The adsorption of Cr(VI), Ni(II) and Cu(II) ions on to Riverbed Sand at three different temperatures were studied obviously he adsorption efficiency decreases as temperatures increases. However the adsorption capacity of heavy metal ions decreased with increasing temperature which indicated that that he adsorption of heavy metal ions were exothermic process. Further adsorption of heavy metal ions was favoured at lower temperature [49].

Adsorption isotherms

Four theoretical isotherm models Langmuir, Freundlich, Tempkin and Dubinin-Radhuskavich were used to explore and analyze the sorption mechanism of Riverbed Sand. The Langmuir model is based on the assumption of surface homogeneity such as equally available adsorption monolayer surface covered. No forces exist between adsorbed molecules on the surface of solid. The linear form of the Langmuir isotherm model is expressed as follows [50, 51].

$$\frac{C_e}{q_e} = \frac{1}{K_L q_m} + \frac{C_e}{q_m} \quad (5)$$

Where K_L is the Langmuir constant related to the energy of adsorption and q_m is the maximum adsorption capacity (mg/g). The graph C_e/q_e against C_e was shown in Fig. 12. The values of q_m and K_L are found from the slope and intercept of the plot and are mention in Table 2. The important characteristics of the Langmuir isotherm can be expressed by the equilibrium parameter R_L, which absolutely decides the favourability and mature of the isotherm of the adsorption process by the following equation:

$$R_L = \frac{1}{1 + K_L C_0} \quad (6)$$

Where *Co* is the initial Cr(VI), Ni(II) and Cu(II) concentration and K_L is the Langmuir adsorption constant (L/mg). The value confirms the adsorption to be unfavourable (R_L<1), linear (R_L=1), favourable (0<R_L<1) or irreversible (R_L=0) [52]. The values of R_L for Cr(VI), Ni(II) and Cu(II) was greater than zero and less than unity which indicated the favourable adsorption of Cr(VI), Ni(II) and Cu(II) on Riverbed Sand. Freundlich isotherm is an empirical model that considers multilayer sorption heterogeneous adsorptive energies on the surface of the adsorbent and can be described as equation: [53].

$$\log q_e = \log K_f + \frac{1}{n} \log C_e \quad (7)$$

Where q_e (mg/g) is the amount of Cr(VI), Ni(II) and Cu(II) adsorbed on the surface of adsorbents at equilibrium and K_f and n are Freundlich constants related to the adsorption intensity and adsorption capacity relatively. Fig. 13. represents graphically the relation between logC_e and logq_e for Cr(VI), Ni(II) and Cu(II) and the values are presented in Table 2. However the results are not fitted well with the Freundlich isotherm according to analysis.

Table 2: Parameters of various isotherms for Cr(VI), Ni(II) and Cu(II) adsorption by Riverbed Sand.

Isotherm	Parameters	Cr(VI)	Ni(II)	Cu(II)
Langmuir	R^2	0.9981	0.9954	0.9944
	q_e (mg/g)	9.803	8.928	7.936
	R_L	0.0383	0.01452	0.0186
	B (l/mg)	2.5063	6.7842	5.274
Freundlich	R^2	0.9885	0.9247	0.9086
	n	3.031	2.2893	2.2558
	K_f [(mg/g)(mg^{-1})$^{1/n}$]	3.9832	2.5587	2.2331
Tempkin	R^2	0.8911	0.8111	0.8745
	B(kJ/mol)	29463.6	4409.4	4925.97
	A (L/mg)	248.042	60.831	14.6758
Dubinin–Radushkevich	R^2	0.6299	0.8676	0.7781
	K_D	2 x 10^{-8}	1 x 10^{-8}	1 x 10^{-8}
	E (kJ/mol)	5	7.07	7.07

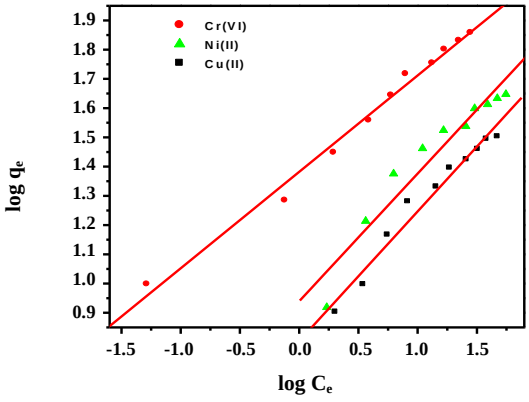

Fig. 13: Linear plot of Freundlich isotherm for adsorption of Cr(VI), Ni(II) and Cu(II) onto Riverbed Sand.

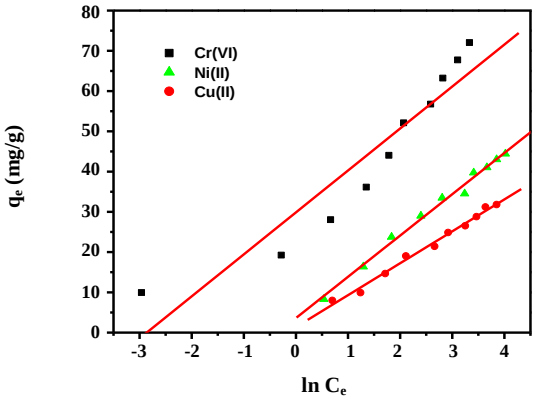

Fig. 14: Linear plot of Temkinisotherm for adsorption of Cr(VI), Ni(II) and Cu(II) onto Riverbed Sand.

The value of Freundlich constant n larger than 1 points out the favourable sorption conditions.

Tempkin isotherm

This isotherm describes the behaviour of adsorption systems on heterogeneous surface and it has generally been applied in the following form [54]:

$$q_e = B \ln A + B \ln C_e \quad (8)$$

Where $B = \frac{RT}{b}$, T is the absolute temperature in kelvin and R is the universal gas constant (8.314 JK/mol) the value of B and A were calculated from the plot of q_e against $\ln C_e$ (Fig. 14) was shown in Table 2. Tempkin isotherm equation assumes that the heat of adsorption of all the molecules in the layer decreases linearly with coverage due to adsorbent-adsorbate interactions and that the adsorption is characterized by a uniform distribution of the binding energies up to some maximum binding energy.

Dubnin – Radushkevich isotherm

Dubnin – Raduskevich isotherms generally applied to express the adsorption mechanism with a Gaussian energy distribution on to a heterogeneous surface. The model has often successfully fitted high solute activities and

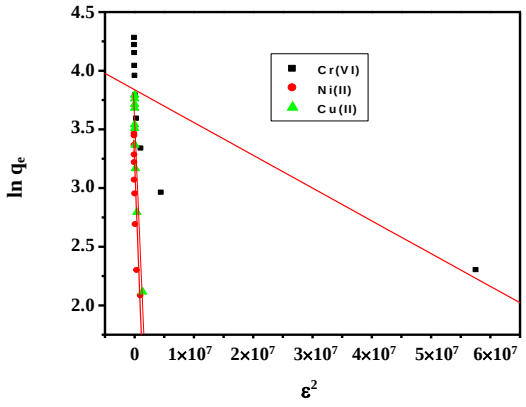

Fig. 15: Linear plot of D – R isotherm for adsorption of Cr(VI), Ni(II) and Cu(II) onto Riverbed Sand.

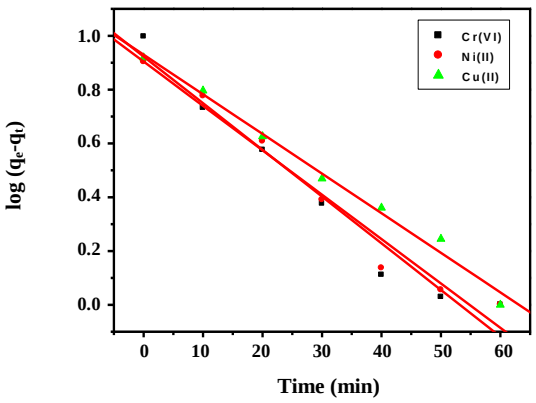

Fig. 16: Pseudo first order kinetics for adsorption of Cr(VI), Ni(II) and Cu(II) onto Riverbed Sand.

the intermediate range of concentration data. The linear form of D-R isotherms is presented as the following equation: [55].

$$\ln q_e = \ln q_m - K_D \varepsilon^2 \quad (9)$$

Where q_e is the amount of Cr(VI), Ni(II) and Cu(II) ions adsorbed per unit mass of adsorbent (mg/g), q_m is theoretical isotherm saturation capacity (mg/g), K_D is the constant of the sorption energy (mol^2/J^2) and ε is polanyi potential, which is described as

$$\varepsilon = R\,T \ln\left(1 + \frac{1}{C_e}\right) \quad (10)$$

Where T is the solution temperature (K) and R is the gas constant and is equal to 8.314 J/mol K. Where q_m is the maximum sorption capacity of the adsorbent (mg/g), ε is the Polanyi sorption potential and K_D (mol^2/J^2) is a constant related to the mean energy of sorption per mole of adsorbate as it is transferred from the bulk solution to the surface of the solid. Plots of $\ln q_e$ vs ε^2 are shown in Fig. 15. The energy E is determined by the following equation:

$$E = \frac{1}{\sqrt{2K_D}} \quad (11)$$

It is known that magnitude of apparent adsorption energy E is useful for estimating the type of adsorption and if this value is below of 8 KJ/mol the adsorption type can be explained by physical adsorption, between 8 and 26 KJ/mol the adsorption type can be explained by ion exchange and over 16 KJ/mol the adsorption type can be explained by a stronger chemical adsorption than ion exchange. The value of E for Cr(VI), Cu(II) and Ni(II) is found to be above 16 KJ/mol (Table 2) which corresponding to chemical adsorption. The comparison of correlation coefficients (R^2) of the linearized form of all the equation indicates that the Langmuir model yields a better fit for the experimental equilibrium adsorption data.

Kinetics studies

Adsorption kinetics has been examined for the purpose to obtain an understanding how the metal ions move rapidly from solution to the adsorbent as well as the removal time needed to reach equilibrium. The kinetic models of adsorption were determined with two most commonly used and known rate equations: pseudo first order (the most reliable kinetics equation suitable only for the rapid initial phase Equation 12) and pseudo second order (for predicting the kinetics behaviour of chemical sorption as a rate controlling step Equation 13) models are expressed as

$$\log\left(q_e - q_t\right) = \log q_e - \frac{K_1}{2.303}.t \quad (12)$$

$$\frac{t}{q_t} = \frac{1}{K_2 q_e^2} + \frac{1}{q_t}.t \quad (13)$$

Where q_e and q_t are the amounts of metals adsorbed (mg/g) at equilibrium and at time t (min) respectively. K_1 (min^{-1}) is the rate constant of pseudo-first order. The linear relation among the value of log (q_e-q_t) versus t reveals the applicability of this model (Fig. 16) [56]. K_2 and the equilibrium adsorption amount (q_e) were measured from the slope and intercept of the plot of t/q_t versus t (Fig. 17) [57, 58]. Where k_2 (g/(mg min))is the rate constant of pseudo-second order kinetic model. h is known as initial sorption constant. The value of $k_1$was determined from

Table 3: Parameters of adsorption kinetic modelsofCr(VI), Ni(II) and Cu (II) onto Riverbed Sand.

Adsorption kinetic model	Parameter	Cr(VI)	Ni(II)	Cu(II)
Pseudo-First order	R^2	0.91	0.9038	0.9011
	k_1 (min^{-1})	0.04007	0.1547	0.1338
	q_e(mg/g)	2.5166	1.8738	1.0555
Pseudo-Second order	R^2	0.9966	0.9982	0.9969
	K_2 (min^{-1})	7.54 x 10^{-3}	6.373 x 10^{-3}	1.522 x 10^{-3}
	q_e(mg/g)	9.7556	8.6505	7.3746
Intraparticle diffusion model	R^2	0.9893	0.9691	0.9688
	K_{diff}	1.2945	0.9264	1.206
	C	0.4613	0.6211	0.6262

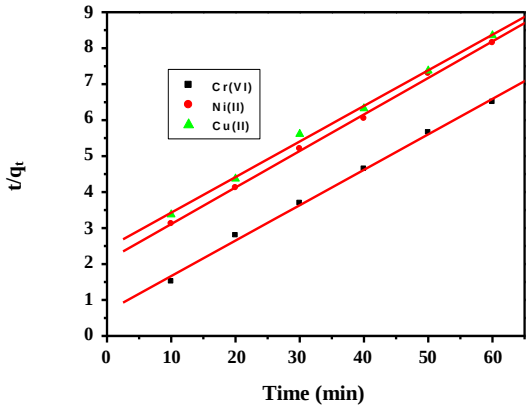

Fig. 17: Pseudo second order kinetics for adsorption of Cr(VI), Ni(II) and Cu(II) onto Riverbed Sand.

the slope of the linear plots of log (q_e-q_t) vs t for Cr(VI), Cu(II) and Ni(II). The initial adsorption rate consultants can be calculated from the pseudo second order model using the equation:

$$h = K_2 q_e^2 \qquad (14)$$

The experimental kinetic study results are shown in Table 3. The high correlation coefficient values of pseudo second order model (R^2= 0.9966 for Cr(VI), 0.9982 for Ni(II) and 0.9969 for Cu(II) over whole adsorption stage in addition to the closeness of theoretical and experimental q_e value show the applicability of this model for analyzing experimental data. The observed result show that the pseudo second order rate equation is good and applicable candidate for explanation of experimental data. Therefore the adsorption kinetics follows the pseudo second order model suggesting a chemisorption process.

Intraparticle diffusion model was used to highlight the rate limiting step of the adsorption process as recommended by *Weber* and *Morris* [59]. If the plot q_t versus $t^{1/2}$ makes a straight line and goes through the origin intraparticle diffusion is the source of the rate limiting step. The equation can be expressed as

$$q_t = K_{id} t^{1/2} + C \qquad (15)$$

Where q_t is the adsorption at any time t, k_{id} is the intraparticle diffusion rate constant and Cis the film thickness. From Fig. 18. the calculated k_{id}, C and the correlation coefficient (R^2) values are tabulated in Table 3. The value of q_t values $t^{1/2}$ and the rate constant k_{id} directly evaluation from the slope of the regression line. The values of provide information about the thickness of the boundary layer and the external mass transfer resistant when adsorption mechanism follows the sole intraparticle diffusion process that impress the plot to cross origin. The values of diffusion rate constants for Cr(VI), Ni(II) and Cu(II) were given in Table 3. The higher the k_{id} values indicated that the faster adsorption of Cr(VI), Ni(II) and Cu(II) from the bulk phase to the exterior surface of QKCI and inside the interior pore. The high value of R^2 confirm the suitability of this model and fact that the rate limiting step is the intraparticle diffusion process.

Adsorption thermodynamics

In order to describe the thermodynamics behaviour of the adsorption of Cr(VI), Ni(II) and Cu(II) ions onto Riverbed Sand ,thermodynamics parameters including the changing of free energy (ΔG°) enthalpy (ΔH°) and entropy (ΔS°) were calculated from the following equation.

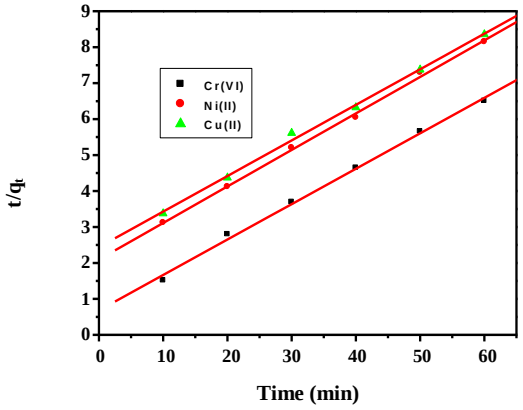

Fig. 18: Intra-particle diffusion model for adsorption of Cr(VI), Ni(II) and Cu(II) onto Riverbed Sand.

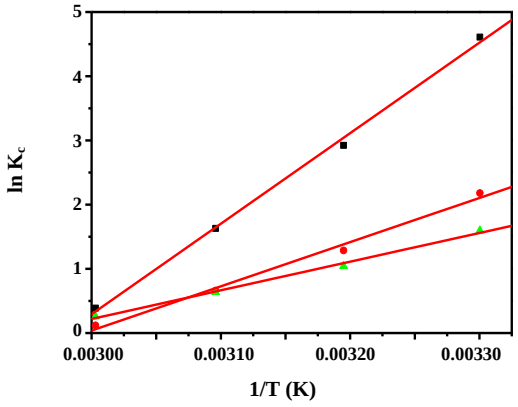

Fig. 19: Van't Hoff plot for the adsorption of Cr(VI), Ni(II) and Cu(II) onto Riverbed Sand.

$$\Delta G^{\circ} = -RT \ln K_D \quad (16)$$

$$\Delta G = \Delta H - T\Delta S \quad (17)$$

$$K_D = \frac{C_0}{C_e} \quad (18)$$

Where K_D is the equilibrium constant C_o and C_e are the Cr(VI), Ni(II) and Cu(II) ions concentration (mg/L) on the adsorbent and in the solution at equilibrium respectively. The plot of ln K_D verses 1/T is presented in Fig. 19 should give a straight line. ΔH^0 and ΔS^0 were calculated from the slope and the intercept of the plots. All the values and coefficients are listed in Table 4 shows Cr(VI), Ni(II) and Cu(II) adsorption follows exothermic path. The decrease in adsorption of metal ions with temperature may be attributed to excess energy supply that promotes desorption. A negative standard enthalpy change suggests that the interaction of Cr(VI), Ni(II) and Cu(II) ions onto Riverbed Sand is exothermic. The negative ΔG^0 values in each individual temperature indicated that thermodynamically adsorption is feasible and spontaneous. The positive value of ΔS^0 reveals the increased random ness at the solid solution interface during the fixation of ion on adsorbent surface.

Comparison with other adsorbent

Various clay and sand based adsorbent for removal of single metal ion removal, including activated clay, modified sand and Riverbed Sand were reported in literature [60-67].The triple metal (Cr(VI), Ni(II) and Cu (II)) adsorption capacity (value of qm derived from Langmuir equation) of Riverbed Sand compared with other sand based adsorbent reported elsewhere and presented in Table 5.

Desorption test

The plausibility of reusing regular adsorbents on different occasions expands the allure of the adsorption procedure. A significant component of the procedure is the advancement of a viable strategy for the recovery of the materials utilized. For this reason a desorption test was completed, utilizing water and hydrochloric acid as the recovering agent. The outcomes exhibited in Table 6 show that water is a powerless desorbing agent. This is proof of a solid bond between the adsorbate and adsorbent. Just when hydrochloric acid was utilized a significant increment in the level of desorption accomplished. It was discovered that as the centralization of the hydrochloric acid utilized as a desorbing agent expanded, there was an improvement in the viability of the adsorbent recovery process. The instrument of desorption depends on the trading of hydrogen ions (H^+) with the adsorbed metal particles. After recovery, the sorbent could be utilized again in further adsorption tests

Optimization of ANN

An ANN was used for modelling the adsorption studies of Cr(VI), Ni(II) and Cu(II) ions. Experimental data obtained under different operating condition were used to train and test the neural network model. In the present work, ANN modelling was performed using MARLAB®R 2011a (The Math works, Inc, U.S) mathematical software by neural network toolbox. A three layer feed-forward

Table 4: Thermodynamic parameters for adsorption of Cr(VI), Ni(II) and Cu (II) onto Riverbed Sand.

Temperature (K)		ΔG°(kJ/mol^{-1})	ΔH° (kJ/mol^{-1})	ΔS° (JK^{-1} mol^{-1})	K_D
Cr(VI)	303	-9.26259	-117.235	349.27	39.52304
	313	-7.60732			18.60307
	323	-4.37475			5.099142
	333	-1.07477			1.47433
Ni(II)	303	-5.49	-57.244	171.409	8.842871
	313	-3.346			3.617808
	323	-1.77			1.936354
	333	-0.330			1.126809
Cu(II)	303	-3.92	-37.105	109.49	4.924873
	313	-2.64			2.831564
	323	-1.67			1.889171
	333	-0.69			1.293736

Table 5: Comparison of adsorption capacities and adsorbates of different adsorbents with Riverbed Sand.

Adsorbent materials	Metal ions	Adsorption capacity (mg g^{-1})	Reference
Tannin-immobilized activated clay	Cr(VI)	24.09	61
Spent activated clay	Cr(VI)	1.422	62
Natural clay	Cr(VI)	10.9	63
Monmorillonite supported magnetic nanoparticles	Cr(VI)	15.3	64
HDTMA modified montmorillonite	Cr(VI)	21.05	65
Modificed sand	Cr (VI)	0.79	66
Riverbed Sand	Cr (VI)	0.15	67
Modified Riverbed Sand	Ni (II)	0.86	68
Riverbed Sand	Cr (VI), Ni(II), Cu (II) (10 mg/L)	9.803, 8.928, 7.936	Present work

Table 6: Desorption of Cr(VI), Ni(II) and Cu (II) ions from the Riverbed Sand using H_2O and HCl.

Metal Ion	Desorption Percentage	
	H_2O	HCl
Cr(VI)	2.5	98.2
Ni(II)	3.2	96.4
Cu(II)	1.4	95.8

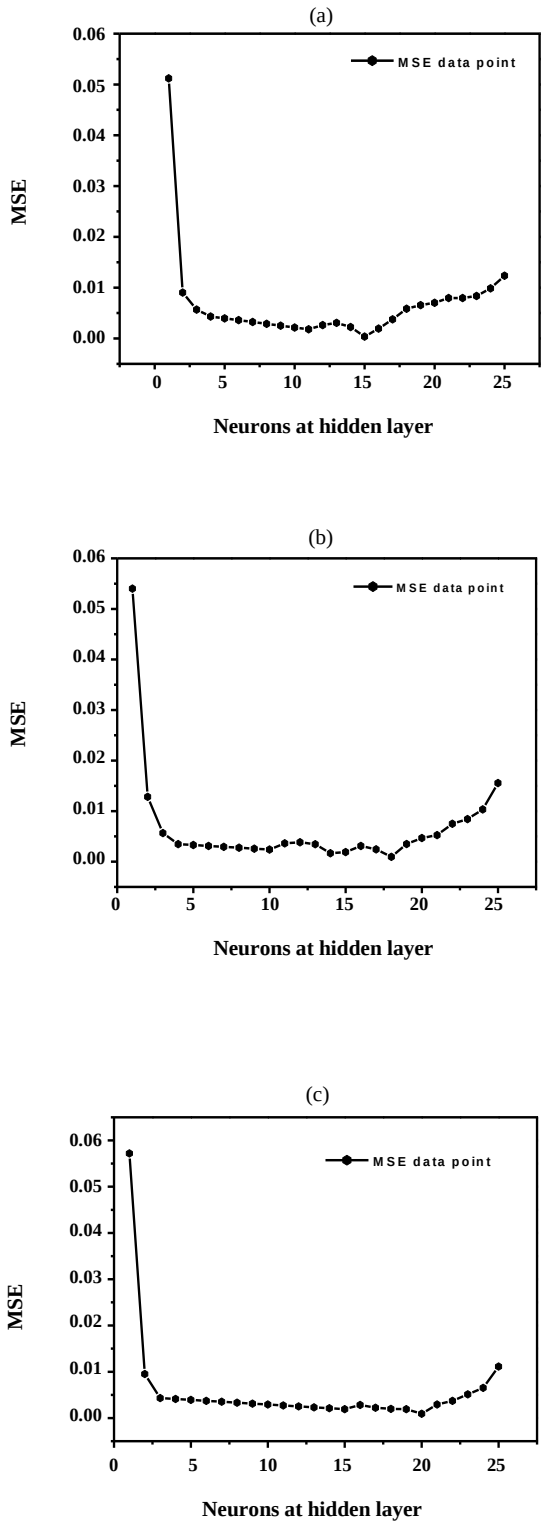

Fig. 20: Dependence between MSE and number of neurons at hidden layer: (a) Cr(VI), (b) Cu(II) and Ni(II).

back propagation neural network consists of input, output and intermediate hidden layers with tangent sigmoid transfer function (tansig) at the hidden layer and an linear transfer function (purelin) at the output layer was used for modelling of the Cr(VI), Ni(II) and Cu(II) ions adsorption capacity. The judgment about the efficiency of ANN model is based on the maximization of R^2 value and reducing the MSE value of the testing set. In network optimization 1 to 30 neurons were utilized in the hidden layer. Each topology was repeated three times to avoid random correlation due to random initialization of weights. We can see that the performance of the network stabilized after inclusion of an adequate number of hidden units. It was found that ANN containing 15, 18 and 20 hidden neuron was chosen as the best models for the removal of Cr(VI), Ni(II) and Cu(II) by QKCI. Respectively using the optimal ANN model the R^2 for the test data set were 0.9866, 0.9649 and 0.9478 (Fig. 20); MSE values were 0.00036, 0.00076 and 0,00092 for Cr(VI), Ni(II) and Cu(II) respectively. During training the weight are updated according to the following equation

$$W_{K+1} = -[J^T(W_K)^J(W_K) + m_K^I]^{-1} \times J^T(W_K)^V(W_K) \quad (19)$$

Where W_{K+1} and W_K are the weight matrix in $K+1^{th}$ and K^{th} iterations, respectively. J is the Jocobian matrix with which it can avoid computing the hessia matrix. V is the cumulative error vector. I is the identity unit matrix. μ_x is a useful feature which allows L_M to switch smoothly between the steepest descent algorithm and Gussain neuron algorithm [68]. Fig. 21 a, b and c illustrated the training, validation and test mean squared error for the Lavenberg-Marquardt algorithm for Cr(VI), Cu(II) and Ni(II) ions respectively. A regression analysis of the network response between ANN outputs and the corresponding targets was performed. Fig. 22 a, b and cshows the relationship between the number of neuron number at hidden layer and MSE for the LM algorithm corresponding to Cr(VI), Ni(II) and Cu(II) ions adsorption. Fig. 23 a, b and c displays a comparison between calculated and experimental values of the output variable for data set by using neural network model. Plot in this figure has correlation coefficient of 0.986, 0.9591 and 0.9469 for Cr(VI), Ni(II) and Cu(II). A correlation coefficient of this plot indicates the reliability of the model.

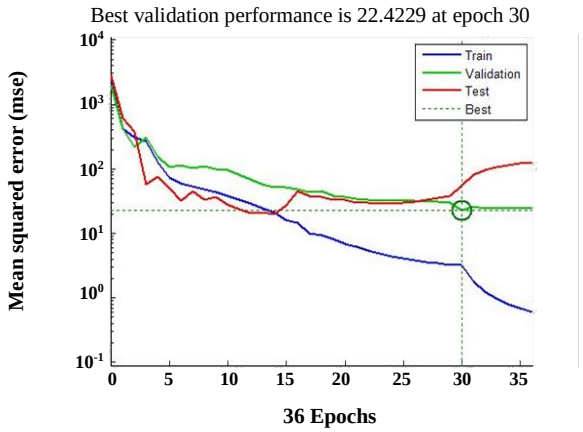

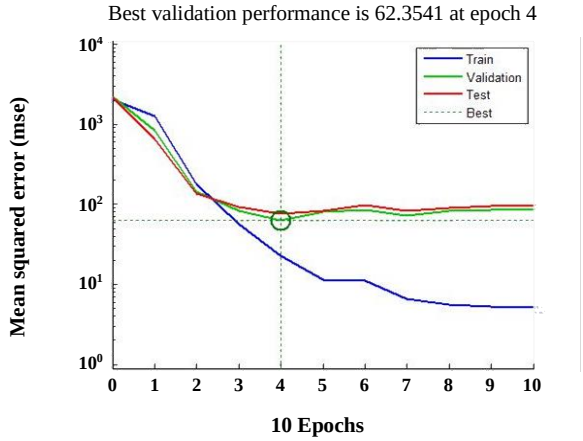

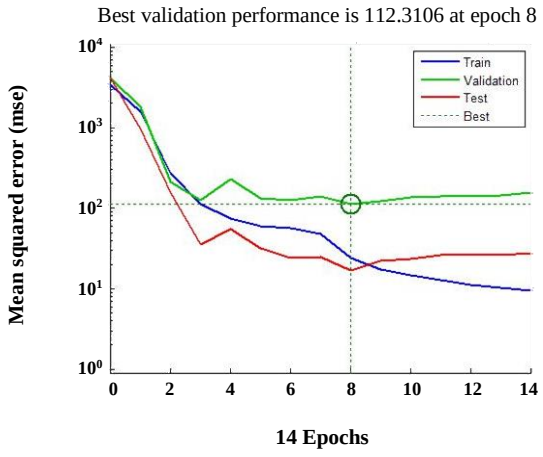

Fig. 21: ANN model training, validation and test mean squared error for Levenberg – Marquardt algorithm: (a) Cr(VI), (b) Cu(II) and Ni(II).

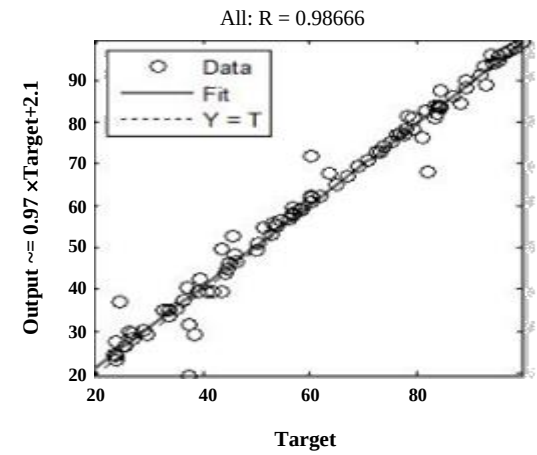

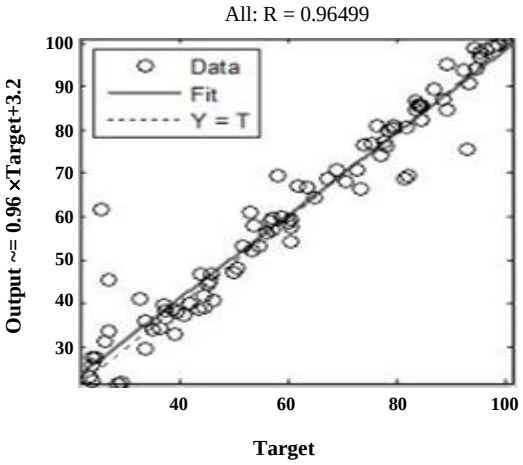

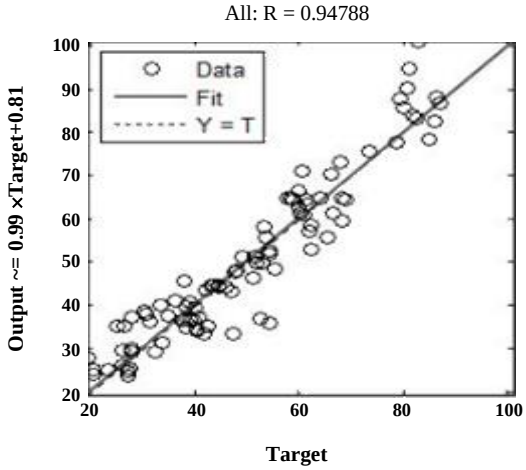

Fig. 22: Regression analysis for adsorption of (a) Cr(VI), (b)Cu(II) and (c) Ni(II).

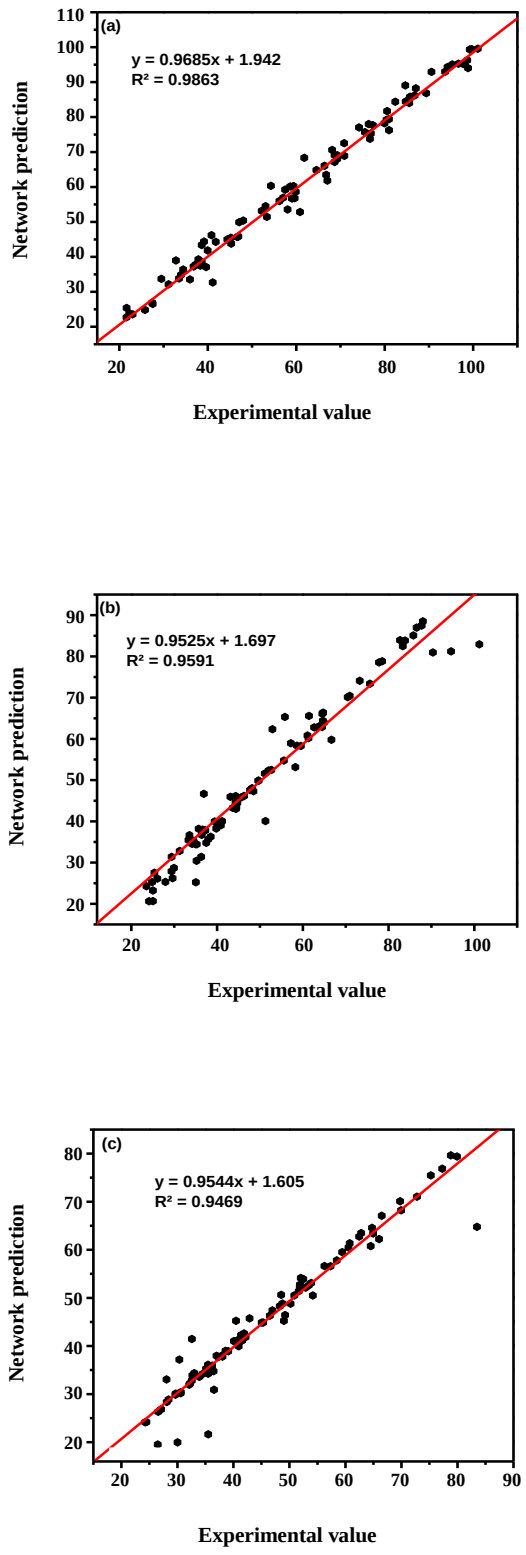

Fig. 23: The experimental data versus predicted data of removal percentage (a) Cr(VI), (b) Cu(II) and (c) Ni(II).

CONCLUSIONS

Riverbed Sand adsorbent have been employed for the removal of Cr(VI), Ni(II) and Cu(II) from aqueous solution in batch mode adsorption experiments. Riverbed Sand was characterized by FT-IR, XRD, SEM, EDAX and N_2 adsorption desorption isotherm techniques. The kinetics and mechanism of adsorption were determined to agree with the pseudo-second order and intra particle diffusion kinetic model. In adsorption the equilibrium adsorption data were found best fit the Langmuir adsorption isotherm suggesting monolayer coverage sorption of Cr(VI), Ni(II) and Cu(II) ions on the surface of Riverbed Sand. Thermodynamic properties signify that the adsorption reaction was spontaneous and exothermic. The traditional feed forward back propagation with the LM training was taken into account for Cr(VI), Ni(II) and Cu(II) ion removal. As a result the algorithm was found to be best with the low MSE and highest R^2. The study indicated that the ANN technique has a great potential in optimization of Cr(VI), Ni(II) and Cu(II) removal efficiency in adsorption process.

Received : Oct. 28, 2019 ; Accepted :Jan. 23, 2020

REFERENCES

[1] Ghosh A., Pal M., Biswas K., Ghosh U.C., Manna B., Manganese Oxide Incorporated Ferric Oxide Nanocomposites (MIFN): a Novel Adsorbent for Effective Removal of Cr (VI) from Contaminated Water, *J. Water Process Eng.*, **7**: 176-186 (2015).

[2] Dubey R., Bajpai J., Bajpai A.K., Green Synthesis of Graphene Sand Composite (GSC) as Novel Adsorbent for Efficient Removal of Cr (VI) Ions from Aqueous Solution, *J. Water Process Eng.*, **5**: 83–94 (2015).

[3] Wu F.C., Tseng R.L., Juang R.S., Kinetic Modeling of Liquid-Phase Adsorption of Reactive Dyes and Metal Ions on Chitosan. Water Res., **35**: 613-618 (2001).

[4] Zhou L., Wang Y., Liu Z., Huang Q., Characteristics of Equilibrium, Kinetics Studies for Adsorption of Hg(II), Cu(II), and Ni(II) Ions by Thiourea-Modified Magnetic Chitosan Microspheres, *J. Hazard. Mater.* **161**: 995–1002 (2009).

[5] Xiong C.H., Li Y.L., Wang G.T., Fang L., Zhou S.G., Yao C.P., Chen Q., Zheng X.M., Qi D.M., Fu Y.Q., Zhu Y.F., Selective Removal of Hg(II) with Polyacrylonitrile-2-Amino-1,3,4- Thiadiazole Chelating Resin: Batch and Column Study. *Chem. Eng. J.*, **259**:257-265 (2015).

[6] Wang X., Lou Y., Ye X., Chena X., Fang L., Zhai Y., Zheng Y., Xiong C., Green Chemical Method for the Synthesis of Chromogenic Fiber and its Application for the Detection and Extraction of Hg^{2+} And Cu^{2+} in Environmental Medium, *J. Hazard. Mater.*, **364**: 339–348(2019).

[7] Qiu J., Wang Z., Li H., Ling X., Jing P., Zhai M., Adsorption of Cr(VI) Using Silica-Based Adsorbent Prepared by Radiation-Induced Grafting, *J. Hazard. Mater*., **166**: 270–276 (2009).

[8] EI-Shafey E.I., Cox M., Pichigin A.A., Appleton Q., Application of a Carbon Sorbent for the Removal of Cadmium and other Heavy Metal Ions from Aqueous Solution, *J. Chem. Technol. Biotechnol.* **77**(4): 429-436 (2002).

[9] Langeroodi N.S., Safaei E., Carbonized Medlar-Core Particles as a New Biosorbent for Removal of Cu^{2+} from Aqueous Solution and Study of its Surface Morphology, *Water Sci. Technol.*, **74**(1): 236-245 (2016).

[10] Langeroodi N.S., Safaei E., Investigation of Removal of Cu (II) Ions by Commercial Activated Carbon: Equilibrium and Thermodynamic Studies, *Prot. Met. Phys. Chem. Surf.*, **55** (1): 28-33 (2019).

[11] Bhattacharya K.G., Gupta S.S., Adsorptive Accumulation of Cd(II), Co(II), Cu(II), Pb(II), and Ni(II) from Water on Montmorillonite: Influence of Acid Activation, *J. Colloid. Interface Sci.*, **310**: 411-424 (2007).

[12] Gottipati R., Mishra S., Process Optimization of Adsorption of Cr (VI) on Activated Carbons Prepared from Plant Precursors by a Two-Level Full Factorial Design, *Chem. Eng. J.*, **160**: 99-107 (2010).

[13] Zhou S., Xue A., Zhang Y., Li M., Li K., Zhao Y., Xing W., Novel Polyamidoamine Dendrimer-Functionalized Palygorskite Adsorbents with High Adsorption Capacity for Pb^{2+} and Reactive Dyes, *Appl. Clay Sci.*, **107**: 220-229 (2015).

[14] Lata H., Garg V.K., Gupta R. K., Sequestration of Nickel from Aqueous Solution onto Activated Carbon Prepared From Parthenium Hysterophorus L. *J. Hazard. Mater.*, **157**: 503-509 (2008).

[15] Amuda O.S., Giwa A. A., Bello I. A., Removal of Heavy Metal from Industrial Wastewater Using Modified Activated Coconut Shell Carbon, *Biochem. Eng. J.*, **36**: 174-181 (2007).

[16] Tirtom V. K., Dinçer A., Decerik S., Ayudemir T., Celik A., Comparative Adsorption of Ni(II) and Cd(II) Ions on Epichlorohydrin Crosslinked Chitosan–Clay Composite Beads in Aqueous Solution, *Chem. Eng. J.*, **197**: 379-386 (2012).

[17] Nayak P.S., Singh B.K., Instrumental Characterization of Clay by XRF, XRD and FTIR, *Bull. Mater. Sci.*, **30**(3): 235–238 (2007).

[18] Grim R. E, "Clay Miner.", Mcgraw-Hill Book Co. New York, (1968).

[19] Sarala Thambavani D., Kavitha B., Prediction and Simulation of Chromium (VI) Ions Removal Efficiency by Riverbed Sand Adsorbent Using Artificial Neural Networks, *Int. J. Eng. Sci. Res. Tech.*, **3**: 906-913 (2014).

[20] Sarala Thambavani D., Kavitha B., Removal of Chromium (VI) Ions by Adsorption Using Riverbed Sand From Tamilnadu–A Kinetic Study, *Int. J. Res*., **1** (2014)

[21] Kavitha B., Saralathambavani D., Adsorption of Chromium (VI) Ions by Riverbed Sand from Mullai Periyar, Tamilnadu, *Chem. Sci. Rev. Lett.*, **3**: 847-859 (2014).

[22] Giri A. K., Patel R. K., Mahapatra S.S., Artificial Neural Network (ANN) Approach for Modelling of Arsenic (III) Biosorption from Aqueous Solution by Living Cells of Bacillus Cereus Biomass, *Chem. Eng. J.*, **178**: 15-25 (2011).

[23] Assefi A., Ghaedi M., Ansari A., Hibibi M. H., Momeni M. S., Removal of Malachite Green From Aqueous Solution by Zinc Oxide Nanoparticle Loaded on Activated Carbon: Kinetics and Isotherm Study, *J. Ind. Eng. Chem.*, **20**: 2905-2913 (2014).

[24] Karimi H., Ghaedi M., Application of Artificial Neural Network and Genetic Algorithm to Modeling and Optimization of Removal of Methylene Blue Using Activated Carbon, *J. Ind. Eng. Chem.*, **20**: 2471-2476 (2014).

[25] Khataee A. R., Zarei M., Dehghan G., Ebadi E., Powhassan M., Biotreatment of a Triphenylmethane Dye Solution Using a Xanthophyta Alga: Modeling of Key Factors By Neural Network, *J. Taiwan Inst. Chem. Eng.*, **42**: 380-386 (2011).

[26] Khataee A., Khani A., A Neural Network Approach For Prediction of Main Product Yields in Methanol to Olefins Process, *Int. J. Chem. React. Eng.*, **7**: 1542-6580 (2009).

[27] Khataee A.R., Fathinia M., Zarei M., Izadkhah B., Joo S.W., Modeling and Optimization of Photocatalytic/Photoassisted-Electro-Fenton Like Degradation of Phenol Using a Neural Network Coupled with Genetic Algorithm, *J. Ind. Eng. Chem*, **20**(4): 1852-1860 (2014).

[28] Khataee A.R., Photocatalytic Removal of C.I. Basic Red 46 on Immobilized TiO_2 Nanoparticles: Artificial Neural Network Modeling, *Environ. Technol.*, **30**: 1155 -1168 (2009).

[29] Kavitha B., Sarala Thambavani D., Kinetics, Equilibrium Isotherm and Neural Network Modeling Studies for the Sorption of Hexavalent Chromium from Aqueous Solution by Quartz/Feldspar/ Wollastonite, *RSC Adv.*, **6**: 5837-5847 (2016).

[30] Jamshidi M., Ghaedi M., Dashtian K., Ghaedi A.M., Hajati S., Goudarzi A., Highly Efficient Simultaneous Ultrasonic Assisted Adsorption of Brilliant Green and Eosin B onto Zns Nanoparticles Loaded Activated Carbon: Artificial Neural Network Modeling, *Spectrochim Acta A.*, **153**: 257-267 (2016).

[31] Kiransan M., Khataee A., Karaca S., Sheydaei M., Artificial Neural Network Modeling of Photocatalytic Removal of o Disperse Dye Using Synthesized of ZnO Nanoparticles on Montmorillonite, *Spectrochim. Acta, Part-A.*, **140**: 465-473 (2015).

[32] Rene E. R., Veiga M. C., Kennes C., Experimental and Neural Model Analysis of Styrene Removal From Polluted Air in a Biofilter, *J. Chem. Techol. Biotechnol*. **84**: 941-948 (2009).

[33] Elías A., Ibarra-Berastegi G., Arias R., Barona A., Neural Networks as a Tool for Control and Management of a Biological Reactor for Treating Hydrogen Sulphide, *Bioprocess. Biosyst. Eng.*, **29**: 129-136 (2006).

[34] Movagharnejad K., Nikzad M., Modeling of Tomato Drying Using Artificial Neural Network, *Comput. Elect. Agri.*, **59**: 78-85 (2007).

[35] Sadrzadeh M., Mohammadi T., Ivakpour J., Kasiri N., Separation of Lead Ions from Wastewater Using Electrodialysis: Comparing Mathematical and Neural Network Modeling, *Chem. Eng. J.*, **144**: 431-441 (2008).

[36] Van Der Marel H.M., Beutelspacher H., Atlas of IR Spectroscopy of Clay Minerals Their Admixtures, CNY. Elsevier Science Publication, (1976).

[37] Tuddenham W.M., Lyon R.J.P., Infrared Techniques in the Identification and Measurement of Minerals, *Anal. Chem.*, **32**:1630-1634 (1960).

[38] Gadsen J.A., 1975, Infrared Spectra of Minerals and Related Inorganic Compounds (London: Butler Works)

[39] Shaker M.A., Adsorption of Co(II), Ni(II) and Cu(II) Ions onto Chitosan-Modified Poly(Methacrylate) Nanoparticles: Dynamics, Equilibrium and Thermodynamic Studies, *J. Taiwan Inst. Chem. Eng.* **57**: 111-122 (2015).

[40] Guyo U., Makawa T., Moyo M., Nharingo T., Nyamunda B.C., Mugadza T., Application of Response Surface Methodology for Cd(II) Adsorption on Maize Tassel-Magnetite Nanohybrid Adsorbent, *Journal of Environmental Chemical Engineering*, **3(4)**: 2472-2483 (2015).

[41] Runtti H., Tuomikoski S., Kangas T., Lassi U., Kuokkanen T., Rämö J., Chemically Activated Carbon Residue from Biomass Gasification as a Sorbent for Iron (II), Copper (II) and Nickel (II) Ions, *J. Water Process Eng.*, **4**: 12–24 (2014).

[42] Singh P.N., Tiwary D., Sinha I., Improved Removal of Cr (VI) by Starch Functionalized Iron Oxide Nanoparticles, *J. Environ. Chem. Eng.*, **2**: 2252–2258 (2014).

[43] Zhu Z., Preparation and Characterization of Functionalized Silica Spheres for Removal of Cu(II), Pb(II), Cr(VI) and Cd(II) From Aqueous Solutions, *RSC Adv*., **5**: 28624-28632 (2015).

[44] Mittal A., Mittal J., Malviaya A., Gupta V. K., Adsorptive Removal of Hazardous Anionic Dye "Congo Red" from Wastewater Using Waste Materials and Recovery By Desorption, *J. Colloid Interface Sci.* **340**: 16-26 (2009).

[45] Zhang Z., Shan Y., Wang J., Ling H., Zang S., Gao W., Zhao Z., Zhang H., Investigation on the Rapid Degradation of Congo Red Catalyzed by Activated Carbon Powder Under Microwave Irradiation, *J. Hazard. Mater.*, **147**: 325-333 (2007).

[46] Nasernejad B., Zadeh T., Pour B. B., Bygi M. E., Zamani A., Comparison for Biosorption Modeling of Heavy Metals (Cr (III), Cu (II), Zn (II)) Adsorption from Wastewater by Carrot Residues, *Process Biochem.*, 40: 1319–1322 (2005).

[47] Gupta V. K., Agarwal S., Saleh T.A., Chromium Removal By Combining The Magnetic Properties of Iron Oxide with Adsorption Properties of Carbon Nanotubes, *Water Res.*, **45**: 2207-2212 (2011).

[48] Mane S.M., Vanjara A.K., Sawant M.K., Removal of Phenol from Wastewater Using Date Seed Carbon, *J. Chin. Chem. Soc.*, **52**:1117-1122 (2005).

[49] Monier M., Ayad D.M., Wei Y., Sarhan A.A., Adsorption of Cu(II), Co(II), And Ni(II) Ions by Modified Magnetic Chitosan Chelating Resin, *J. Hazard. Mater.*, **177**: 962–970 (2010).

[50] Langmuir I., The Adsorption of Gases on Plane Surfaces of Glass, Mica And Platinum, *J. Am. Chem. Soc.*, **40**:1361-1430 (1918).

[51] Langeroodi N.S., Farhadravesh Z, Khalaji A.D., Optimization of Adsorption Parameters for Fe (III) Ions Removal from Aqueous Solutions by Transition Metal Oxide Nanocomposite, *Green Chem. Let. Rev.*, **11**(4): 404-413 (2018).

[52] Nasehi S. M., Ansari S., Sarshar M., Removal of Dark Colored Compounds from Date Syrup Using Activated Carbon: a Kinetic Study, *J. Food Eng.*, **111**: 490-495 (2012).

[53] Mittal A., Malviya A., Kaur D., Mittal J., Kurup L., Studies on The Adsorption Kinetics and Isotherms for The Removal and Recovery of Methyl Orange from Wastewaters Using Waste Materials, *J. Hazard. Mater.*, **148**:229-240 (2007).

[54] Gupta S., Babu B.V., Removal of Toxic Metal Cr (VI) from Aqueous Solutions Using Sawdust as Adsorbent: Equilibrium, Kinetics and Regeneration Studies, *Chem. Eng. J.*, **150**:352-365 (2009).

[55] Debey R., Bajpai J., Bajpai A.K., Green Synthesis of Graphene Sand Composite (GSC) as Novel Adsorbent for Efficient Removal of Cr (VI) Ions from Aqueous Solution, *J. Water Process. Eng.*, **2**: 83-94 (2015).

[56] Purkait M.K., Gusain D.S., Das Gupta S., De S., Adsorption Behavior of Chrysoidine Dye on Activated Charcoal and its Regeneration Characteristics by Using Different Surfactants, *Sep. Sci. Technol.* **39(10)**: 2419 – 2440(2005).

[57] Ho Y.S., Mckay G., Pseudo-Second order Model for Sorption Processes, *Process Biochem.*, **34**: 451-465 (1999).

[58] Mirania S., Langeroodi N.S., Goudarzi A., Ebrahimi P., Mn^{2+} Ions Retention onto Agriculture Waste: A Statistical Design Analysis, Estimation of Equilibrium and Kinetic Parameters, *Desalin Water Treat.*, **72**:52-60 (2017).

[59] Weber Jr., W.J., Morris, J.C., Sanit, J., Kinetics of Adsorption on Carbon from Solution, *Journal of The Sanitary Engineering Division, American Society of Civil Engineers*, **89**:31-60 (1963).

[60] Li W., Tang Y., Zeng Y., Tong Z., Liang D., Cui W., Adsorption Behavior of Cr(VI) Ions on Tannin-Immobilized Activated Clay, *Chem. Eng. J.*, **193-194**: 88–95 (2012).

[61] Weng C.H., Sharma Y.C., Chu S.H., Adsorption of Cr(VI) from Aqueous Solutions by Spent Activated Clay, *J. Hazard. Mater.* 155:65–75 (2008).

[62] Eloussaief M., Kallel N., Yaacoubi A., Benzina M., Mineralogical Identification, Spectroscopic Characterization, and Potential Environmental Use of Natural Clay Materials on Chromate Removal From Aqueous Solutions, *Chem. Eng. J.*, **168**:1024–1031 (2011).

[63] Yuan P., Fan M., Yang D., He H., Liu D., Yuan A., Zhu J.X., Chen T.H., Montmorillonite-Supported Magnetite Nanoparticles for the Removal of Hexavalent Chromium [Cr(VI)] from Aqueous Solutions, *J. Hazard. Mater.* **166**:821–829 (2009).

[64] Krishna B.S., Murty D.S.R., Jai Prakash B.S., Surfactant-Modified Clay as Adsorbent for Chromate, *Appl. Clay Sci.*, **20**:65–71 (2001).

[65] Yadav S., Srivastava V., Banerjee S., Weng C.H., Sharma Y.C., Adsorption Characteristics of Modified Sand for the Removal of Hexavalent Chromium Ions from Aqueous Solutions: Kinetic, Thermodynamic and Equilibrium Studies, *Catena*, **100**: 120–127 (2012).

[66] Sharma Y.C., Uma, Srivastava V., Srivastava J., Mahto M., Reclamation of Cr(VI) Rich Water and Wastewater by Wollastonite, *Chem. Eng. J.*, **127**: 151–156 (2007).

[67] Yadav S., Srivastava V., Banerjee S., Gode F., Sharma Y. C., Studies on the Removal of Nickel from Aqueous Solutions Using Modified Riverbed Sand, *Environ. Sci. Pollut. Res*., **20**: 558–567 (2013).

[68] Assefi P., Ghaedi M., Ansari A., Hibibi M.H., Momeni M.S., Artificial Neural Network Optimization for Removal of Hazardous Dye Eosin Y from Aqueous Solution Using Co_2O_3-NP-AC: Isotherm and Kinetics Study, *J. Ind. Eng. Chem.* **20**: 2905-2913 (2014).